Progressive collapse analysis of RC frame building based on Pseudo-Dynamic (PsD) testing with sub-structuring

David Bertrand, Stéphane Grange, J-.B. Charrié

Version of Record: https://www.sciencedirect.com/science/article/pii/S2352710222004338
Manuscript_cf277546f408e22794bd15f0697c7b20

Progressive collapse analysis of RC frame building based on Pseudo-Dynamic (PsD) testing with sub-structuring

D. Bertrand*, S. Grange, and J-.B. Charrié

March 21, 2022

Abstract

Accidental loading coming from either natural or anthropic hazards can have serious consequences on civil engineering structures capacity and can lead to progressive collapse (PC). In the case of frame buildings, PC is a subject of interest to assess the residual risk of exposure to death for people inside. PC analysis on large structures is rather performed from a numerical point of view. Experimental tests are often expensive and complicate to setup (dynamic response, removal of the load-bearing element, size of the experiment, *etc.*). In this paper, the use of Pseudo-Dynamic (PsD) testing combined with sub-structuring technique is proposed. It allows to account for the dynamic response of the entire structure by only testing (*quasi*-statically) the critical part of the building. In order to demonstrate the applicability of the method to PC, a classic central column removal scenario is considered and applied on a Reinforced Concrete (RC) structure. The latter is a two-bay and three story frame building. The bending response of the RC beam directly connected to the removed load-bearing member is investigated. Only this part (the RC beam) is experimentally tested while the rest of the structure is simulated by finite element analysis within a dynamic framework. The *quasi*-static response of the beam is measured and interacts with the integration scheme (α Operator

*Corresponding author : D. Bertrand, david.bertrand@insa-lyon.fr, tel : +33(4) 72 43 72 94, fax : +33 (0)4 72 43 85 21

Splitting type) to calculate, *inter alias*, the inertial forces contributions and the displacement fields within both numerical and experimental domains. To validate the approach, a finite element model based on multifiber beam theory is used. The results comparison underlines a very good agreement between both PsD tests and numerical simulations in all configurations considered, in particular the ability of the PsD approach to account for inertial effects within the structural response. It demonstrates the interest to use such a method within the context of PC analysis. More specifically, the method could prove particularly effective to assess Dynamic Amplification Factors (DAF), used for structural design by accounting for PC potential effect (at least within American guidelines).

Highlights

- Pseudo dynamic testing with sub-structuring applied to progressive collapse
- Dynamic response of RC frame structures subjected to central column removal scenario
- Nonlinear multifiber beam finite element modeling
- Time evolution of crack pattern within concrete measured by Digital Image Correlation (DIC)

1 Introduction

In civil engineering, the sudden loss of vertical load-bearing elements can significantly affect the integrity of a structure and may lead to Progressive Collapse (PC). This topic has a crucial importance for the engineering community, due to the serious consequences (casualties, loss of functionality, *etc.*) associated with the partial or complete collapse of a structure following a localized failure (Krauthammer et al. [2003], Sasani and Kropelnicki [2008], Yagob and Galal [2009]). The interest for PC has drastically increased since the attack of the World Trade Center in 2001 (Bazant and Zhou [2002]). Although an extensive literature on the subject, new knowledge (Adam et al. [2018], Kiakojouria et al. [2020]) and technics (Tian et al. [2020], Meng et al. [2022]) are still needed to propose structures capable of resisting both structurally and functionally to a localized loss of load-bearing members.

The causes of PC can be diverse and varied (gas explosion, fire, natural or anthropic hazards, design defect, *etc.*). Depending on building type and initial location of bearing capacity loss, PC can develop several typologies (Starossek [2007]) which, in some cases, can be threat-dependent (Kiakojouria et al. [2020], Yi et al. [2021]) and underlines the complexity of such a phenomenon.

Approaches to characterize the building's response to localized structural loss of bearing rely on experiments (Alshaikh et al. [2020], Yi et al. [2021]) to validate numerical models (Sasani and Kropelnicki [2008], Byfield et al. [2014], ElHajjDiaba et al. [2021]) and to propose *ad-hoc* guidelines for engineers (AmericanStd [2009], AmericanStd [2016a]). During the previous 20 years, many experiments were developed to investigate buildings' responses to PC. For instance, field full-scale experimental tests were performed (Sasani and Sagiroglu [2008], Song et al. [2010], Wang et al. [2016], Shan et al. [2016] *etc.*). To get a better control on the tested structures, many experiments have been carried out within a laboratory environment. *Quasi*-static experiments on sub-assemblages were often considered (Yi et al. [2008], Lew et al. [2011], Sadek et al. [2011]). Experiments in dynamic conditions were also performed to analyze the dynamic effect of instantaneous removal of the load bearing element on the structure's capacity and on the force redistribution (Kai and Li [2012], Kai and Li [2013], Kai and Li [2014] and Orton and Kirby [2014]). In 2015, a comparison between *quasi*-static and dynamic experiments underlined the need to define Dynamic Amplification Factors (DAF) (Liu et al. [2015]). DAF are used to account for dynamic effects involved

during a PC event where structural analysis is performed under *quasi*-static conditions. Pham and Tan [2017] have shown that DAF's main origin comes from the inertial effect related to rapid loading change during the accidental event. Under the assumption of threat-independent progressive collapse and excepted for the directly exposed structural element (for instance a bearing column which can be subjected to a projectile), the strain rate has a limited effect on the apparent strength of materials. Based on this assumption, the directly exposed element is generally not taken into account, as its bearing capacity can be considered as null.

In addition, from a design point of view, Scalvenzi et al. [2022] underlines that DAF can be used to account for the inertial effect when *quasi*-static approaches are considered. Structures designed following American guidelines can be justified based on DAF expressions. The latter can be found in AmericanStd [2016b], which is not yet the case within the Eurocode framework (EuropeanStd [2014]).

DAF can be determined by a direct comparison of the *quasi*-static and dynamic experimental responses of the considered structure. However, this approach can lead to redhibitory costs. Full-scale experiments are also needed to guarantee representativeness of the results. As noticed by Wang et al. [2014], the experiment size is very often a limiting factor, given the costs and difficulties of implementation (large scale, dynamic solicitation, logistics, *etc.*). This is all the more true when the size of buildings to be tested can be extremely important, whereas the damageable zone is of more modest size.

In this paper, the Pseudo-Dynamic (PsD) approach combined with sub-structuring (Pegon and Pinto [2000] Souid et al. [2009]) is applied to PC analysis, which, to the author's knowledges, has never been done before. This technique consists of testing a part of a structure under *quasi*-static conditions and simulating the rest of the structure accounting for inertial effects in order to get the full dynamic response. By experimentally testing only the part of the structure that is vulnerable and is expected to develop a high degree of damage, PsD sub-structuring tests will resolve the scaling issues to some extent.

In most accidental scenarii leading to PC, the strain rate imposed at the material scale remains low (Pham and Tan [2017], Yi et al. [2021]) and the main part of the dynamics response is governed by inertia. This justifies the use of PsD tests within PC context.

This approach is an excellent alternative to the current techniques used in PC analysis. PsD tests are easier to perform than dynamic ones (low data

acquisition frequency, time dilation, *etc.*) because only *quasi*-static tests are performed. Cost is reduced and experimental implementation is facilitated. It allows considering a repetition of experiments in order to explore the parameter space with a good degree of control and confidence, accounting for inertial effects on a full scale structure.

Many configurations of framed structures can be considered, combined with multiple accidental senarii (central or corner column removal, multiple removals, single or multiple removals, multiple bay and story frame, *etc.*). As a demonstrator of the potential of the method, a classic threat-independent center column removal scenario is considered. The structure is a two-bay and three-story 2D RC frame.

The first part of the paper presents the PsD test combined with a sub-structuring approach. Then, the accidental scenario is exposed and the idealized frame structure is detailed. The tested critical part is a RC beam subjected to an instantaneous removal of its central load-bearing column. Then, the experimental protocol and the instrumentation used are presented. Four RC beams are tested under *quasi*-static and dynamic pushovers, and PsD conditions. Next, a multifiber finite element model is setup and used to compare numerical and experimental results. The latter allows describing the nonlinear response of the RC beam and its effect onto the rest of the structure. Finally, the results are discussed.

2 Material and Methods

2.1 Pseudo-Dynamic testing with sub-structuring

The PsD approach has been widely used to test civil engineering structures subjected to earthquake loading. Generally speaking, earthquakes generate small loading rates compared to impact or blast scenarii and, for non-sensitive materials to strain rate, only inertial effects are involved in the dynamic response of the structure. The main idea of the PsD testing is to solve through time the motion equation using the *quasi*-static structure's response, and simulating the inertial effects involved by mass acceleration. It requires the use of an *ad hoc* time integration scheme. The combination of the PsD approach with sub-structuring technique allows to test a single part of a structure, and to simulate the rest using the finite element method (FEM). In the next paragraph, the classic PsD method (without sub-structuring) is

presented, and then extended with sub-structuring technique.

2.1.1 Pseudo dynamic algorithm used

The α-OS splitting algorithm has been used which is particularly adapted because of its implicit and non-iterative nature (Hilbert et al. [1977], Nakashima and Kato [1987] and Combescure and Pegon [1997]). At time $t_{n+1} = t_n + \Delta t$, (n being the time iteration index), the equation of motion can be written such as

$$\mathbb{M}\boldsymbol{a}^{n+1} + \mathbb{C}\boldsymbol{v}^{n+1} + \boldsymbol{R}^{n+1}(\boldsymbol{d}^{n+1}) = \boldsymbol{F}_{\boldsymbol{ext}}^{\boldsymbol{n+1}} \tag{1}$$

where $\mathbb{M}$ is the mass matrix, $\mathbb{C}$ is the damping matrix, $\boldsymbol{F_{ext}}$ are the external forces applied through time to the structure and $\boldsymbol{R}$ are the restoring forces coming from the static measurements. *Rayleigh* damping is used to define $\mathbb{C}$ such as $\mathbb{C} = \alpha_R\mathbb{M} + \beta_R\mathbb{K}^I$ with $\alpha_R = \frac{2\xi}{\omega_1+\omega_2}$ and $\beta_R = 2\xi\frac{\omega_1\omega_2}{\omega_1+\omega_2}$. $\mathbb{K}^I$ is a stiffness matrix. ω_1 and ω_2 are the pulsations for which the damping ratio is imposed at the value ξ.

$\boldsymbol{d}$ (resp. $\boldsymbol{v}$ and $\boldsymbol{a}$) are the nodal displacements (resp. velocities and accelerations) of the structure. Numerical integration is performed based on a predictor-corrector procedure. First, displacements' prediction (which have to be imposed to the structure) is calculated from the kinematic values obtained at time t_n as

$$\text{Predictor step} \begin{cases} \tilde{\boldsymbol{d}}^{n+1} = \boldsymbol{d}^n + \Delta t\, \boldsymbol{v}^n + \frac{\Delta t^2}{2}\left(1 - 2\beta\right)\boldsymbol{a}^n \\ \tilde{\boldsymbol{v}}^{n+1} = \boldsymbol{v}^n + \Delta t(1-\gamma)\boldsymbol{a}^n \end{cases} \tag{2}$$

$\gamma = (1-2\alpha)/2$ and $\beta = (1-\alpha)^2/4$ are expressed as a function of α, parameter of the α method (Hilbert et al. [1977]). The desired displacements ($\tilde{\boldsymbol{d}}^{n+1}$) are imposed statically to the structure and controlled by measurement ($\tilde{\boldsymbol{d}}_m^{n+1}$) to obtain the gap between the real and desired displacement values. At the same time, the restoring forces are measured ($\tilde{\boldsymbol{R}}_m^{n+1}$). The acceleration is computed at t_{n+1} as

$$\boldsymbol{a}^{n+1} = \hat{\mathbb{M}}^{-1}\hat{\boldsymbol{f}}^{n+1+\alpha} \tag{3}$$

$\hat{\mathbb{M}}$ is the pseudo-mass matrix and $\hat{\boldsymbol{f}}^{n+1+\alpha}$ is the pseudo-force vector, expressed as

$$\left\{\begin{array}{rcl} \hat{\mathbb{M}} = & \mathbb{M} + \gamma\,\Delta t\,(1+\alpha)\,\mathbb{C} + \beta\,\Delta t^2(1+\alpha)\,\mathbb{K}^I \\ \hat{\boldsymbol{f}}^{n+1+\alpha} = & (1+\alpha)\,\boldsymbol{F}_{\boldsymbol{ext}}^{\boldsymbol{n+1}} - \alpha\,\boldsymbol{F}_{\boldsymbol{ext}}^{\boldsymbol{n}} + \alpha\,\tilde{\boldsymbol{R}}^n - (1+\alpha)\tilde{\boldsymbol{R}}^{n+1} + ... \\ & ... + \alpha\,\mathbb{C}\,\tilde{\boldsymbol{v}}^n - (1+\alpha)\,\mathbb{C}\,\tilde{\boldsymbol{v}}^{n+1} + \alpha(\gamma\,\Delta t\,\mathbb{C} + \beta\,\Delta t^2\,\mathbb{K}^I)\boldsymbol{a}^n \end{array}\right. \tag{4}$$

where $\hat{\mathbb{M}}$ involves a stiffness matrix $\mathbb{K}^I$. To guarantee the algorithm's convergence, $\mathbb{K}^I$ has to be chosen as close as possible to the initial elastic stiffness matrix of the tested structure and at least higher than the current tangent matrix (Combescure and Pegon [1997]). In order to assess the value of $\mathbb{K}^I$, preliminary tests are performed. The latter consist to push and release tests where the magnitude of the imposed displacement guarantee than the structure remains within the elastic domain. Then, the value of $\mathbb{K}^I$ is fixed during all the PsD iterative process.To compensate measurement uncertainties and avoid iteration within a time-step, the evaluation of the restoring force at time t_{n+1} is based on an operator splitting, allowing to get the restoring forces' estimation

$$\tilde{\boldsymbol{R}}^{n+1} \approxeq \tilde{\boldsymbol{R}}_m^{n+1} + \mathbb{K}^I\left[\tilde{\boldsymbol{d}}_m^{n+1} - \tilde{\boldsymbol{d}}^{n+1}\right] \tag{5}$$

Then, $\hat{\boldsymbol{f}}^{n+1+\alpha}$ is calculated from the restoring forces ($\tilde{\boldsymbol{R}}^{n+1}$) at time t_{n+1}. Finally, the kinematic field is corrected as

$$\text{Corrector step}\left\{\begin{array}{l} \boldsymbol{d}^{n+1} = \tilde{\boldsymbol{d}}^{n+1} + \beta\Delta t^2\,\boldsymbol{a}^{n+1} \\ \boldsymbol{v}^{n+1} = \tilde{\boldsymbol{v}}^{n+1} + \gamma\Delta t\,\boldsymbol{a}^{n+1} \end{array}\right. \tag{6}$$

2.1.2 Sub-structuring technique

The principle of sub-structuring within the framework of PsD testing is presented in Figure 1. A part of the structure is simulated (noted S), while the critical part is tested (noted T) under *quasi*-static conditions. The same equations are used, but a domain decomposition has to be done in order to separate the simulated and tested parts. The resolution process is based on Pegon and Pinto [2000]. The global system can be written as:

$$\begin{bmatrix} {}^S\hat{M}_{ij} & {}^S\hat{M}_{i\theta} & 0 \\ {}^S\hat{M}_{\delta j} & {}^S\hat{M}_{\delta\theta} + {}^T\hat{M}_{\delta\theta} & {}^T\hat{M}_{\delta J} \\ 0 & {}^T\hat{M}_{I\theta} & {}^T\hat{M}_{IJ} \end{bmatrix} \begin{bmatrix} a_j^{n+1} \\ a_\theta^{n+1} \\ a_J^{n+1} \end{bmatrix} = \begin{bmatrix} {}^S\hat{f}_i^{n+1+\alpha} \\ {}^S\hat{f}_\delta^{n+1+\alpha} + {}^T\hat{f}_\delta^{n+1+\alpha} \\ {}^T\hat{f}_I^{n+1+\alpha} \end{bmatrix} \tag{7}$$

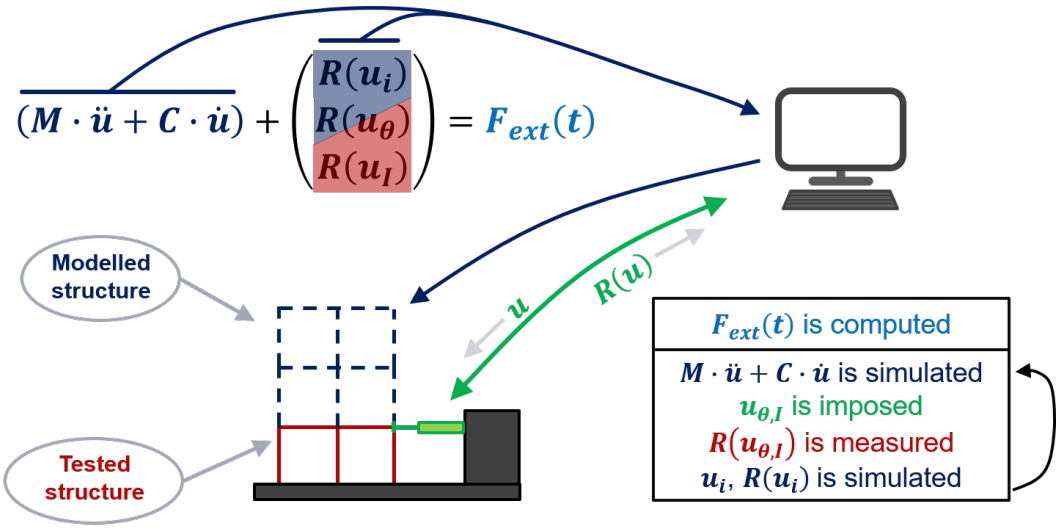

Figure 1: Principle of the Pseudo-Dynamic procedure with sub-structuring. The structure's red part is experimentally tested using jack actuators (in green), whereas the blue part is simulated using the FEM.

The Degrees Of Freedom (DOFs) related to the simulated (resp. tested) part are indexed i and j (resp. I and J). DOFs at the interface are indexed δ and θ. A static condensation is performed to separate the simulated and tested domains from a calculation point of view, to treat each part in parallel. The pseudo-mass matrix is generated independently. Then, accelerations of the modelled part's DOFs (a_j^{n+1}) are condensed onto the tested part. This is given by the first line of the equations system 7.

$$ {}^{S}\hat{M}_{ij} a_j^{n+1} = {}^{S}\hat{f}_i^{n+1+\alpha} - {}^{S}\hat{M}_{i\theta} a_\theta^{n+1} \tag{8} $$

Re-injecting equation (8) within the second and third lines of the equations system (7), the matrix system becomes:

$$ \begin{bmatrix} {}^{T}\hat{M}_{\delta\theta} + {}^{SC}\hat{M}_{\delta\theta} & {}^{T}\hat{M}_{\delta J} \\ {}^{T}\hat{M}_{I\theta} & {}^{T}\hat{M}_{IJ} \end{bmatrix} \begin{bmatrix} a_\theta^{n+1} \\ a_J^{n+1} \end{bmatrix} = \begin{bmatrix} {}^{T}\hat{f}_\delta^{n+1+\alpha} + {}^{SC}\hat{f}_\delta^{n+1+\alpha} \\ {}^{T}\hat{f}_I^{n+1+\alpha} \end{bmatrix} \tag{9} $$

With ${}^{SC}\hat{M}_{\delta\theta} = {}^{S}\hat{M}_{\delta\theta} - {}^{S}\hat{M}_{\delta j} {}^{S}\hat{M}_{ji}{}^{-1} {}^{S}\hat{M}_{i\theta}$ and ${}^{SC}\hat{f}_\delta^{n+1+\alpha} = {}^{S}\hat{f}_\delta^{n+1+\alpha} - {}^{S}\hat{M}_{\delta j} {}^{S}\hat{M}_{ji}{}^{-1} {}^{S}\hat{f}_i^{n+1+\alpha}$. The algorithm is described in the figure 2.

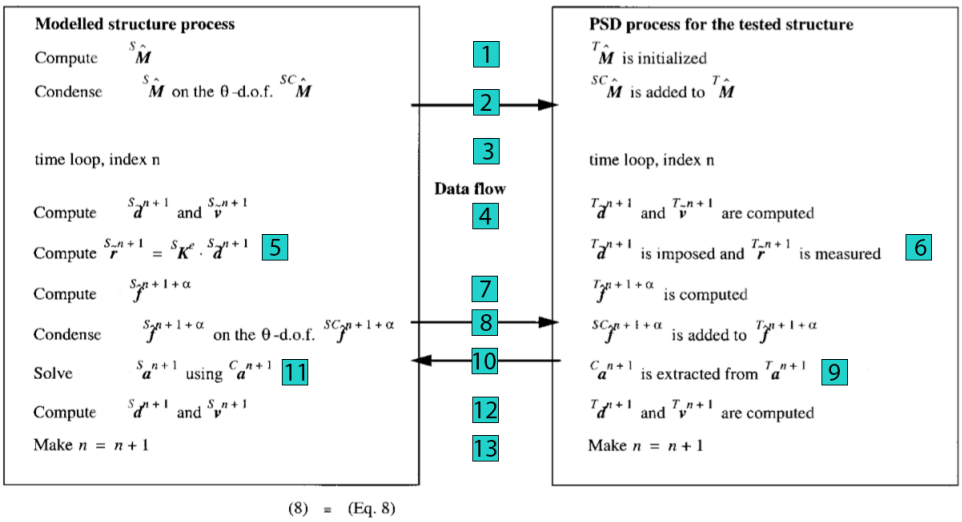

Figure 2: Chronological phases during a time-step of the PsD algorithm combined with sub-structuring proposed by Pegon and Pinto [2000].

2.2 Accidental scenario and structure description

To demonstrate the interest of studying progressive collapse using PsD testing with sub-structuring, an idealized RC structure is considered. The building's robustness to an accidental localized damage is analyzed by considering instantaneous removal of the lower central load-bearing component. In such a case, the most affected members are the horizontal beams, subjected to a significant increase of bending internal efforts.

The initial geometry of the structure is a 2D frame, composed of 4 stories of 2 bays each (Figure 3). The post and beam structure is 4 meters high, and 2.15 meters width. Posts are supposed embedded at the lower ends. In order to exhibit the approach's ability to capture nonlinear responses of tested members, additional masses of 2800 kg each are located at the main nodes. Internal hinges between the two external posts and the floors are also added. The structure's global geometry is presented in figure 4b, as well as the beams' cross-sections, and the internal and external boundary conditions. The structure's tested part is the lower horizontal beam, corresponding to a RC beam.

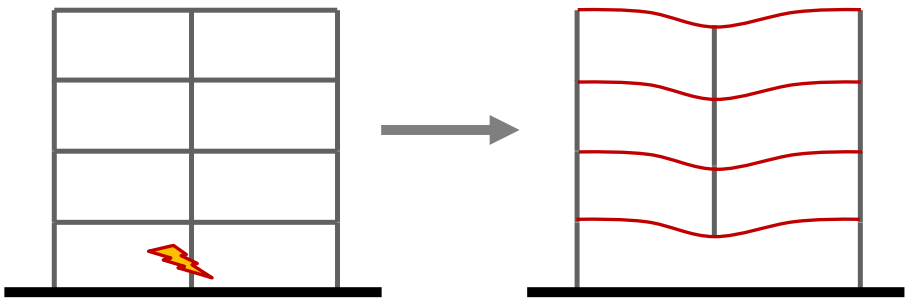

Figure 3: Accidental scenario considered: Instantaneous removal of the central load-bearing element (threat-independent assumption).

2.3 Experimental tests

2.3.1 Tested RC beam features

The RC beam is 230 cm long and has a cross-section of 15 cm×25 cm. A C25/30 concrete class and high strength steel reinforcement are considered. The RC beam is designed following the Eurocode2 recommendations and can support 20 kN (Ultimate Limit State) when subjected to a three-point bending test. Geometry and reinforcement details are depicted in Figure 5.

Four RC beams are cast in place, all according to the specifications above. The concrete's mechanical strength is assessed using 11 cm×22 cm cylindrical samples, tested in compression. These have been cast during the manufacturing of each beam. All tests have been done after at least 28 days of drying.

For the last beam (n^o 4), four additional samples are tested in tension with indirect tensile tests on cylindrical concrete samples. The concrete exhibits a mean compressive strength of 29.8 MPa and a mean tension strength of 2.8 MPa (Figure 6). From the manufacturer specifications, the steel has an elastic limit stress of at least $f_y = 500$ MPa.

2.3.2 Instrumentation

For all tests, the beam's mid-span displacement is recorded by the hydraulic jack actuator's internal sensor. The absolute position error is lower than 0.02 mm. The load applied by the actuator to the structure is measured with a pancake load cell, rated for 100 kN. Its linearity error is lower than 0.2%.

In addition, Digital Image Correlation (DIC) is performed in the Re-

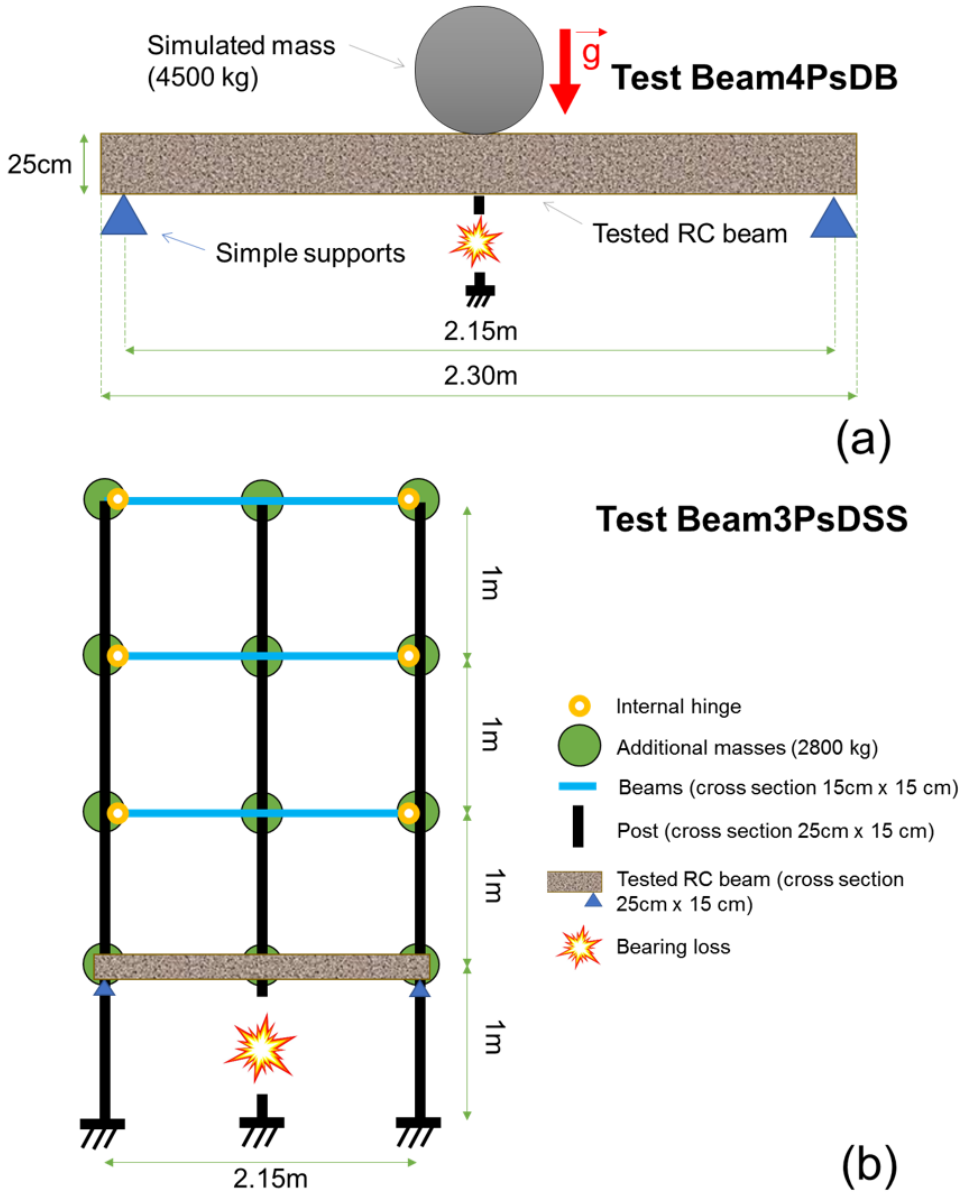

Figure 4: Pseudo-Dynamic testing setups for loss of bearing analysis: Test `Beam4PsDB` without sub-structuring considering a RC beam (a) and Test `Beam3PsDSS` with sub-structuring where the simulated part is considered elastic (b).

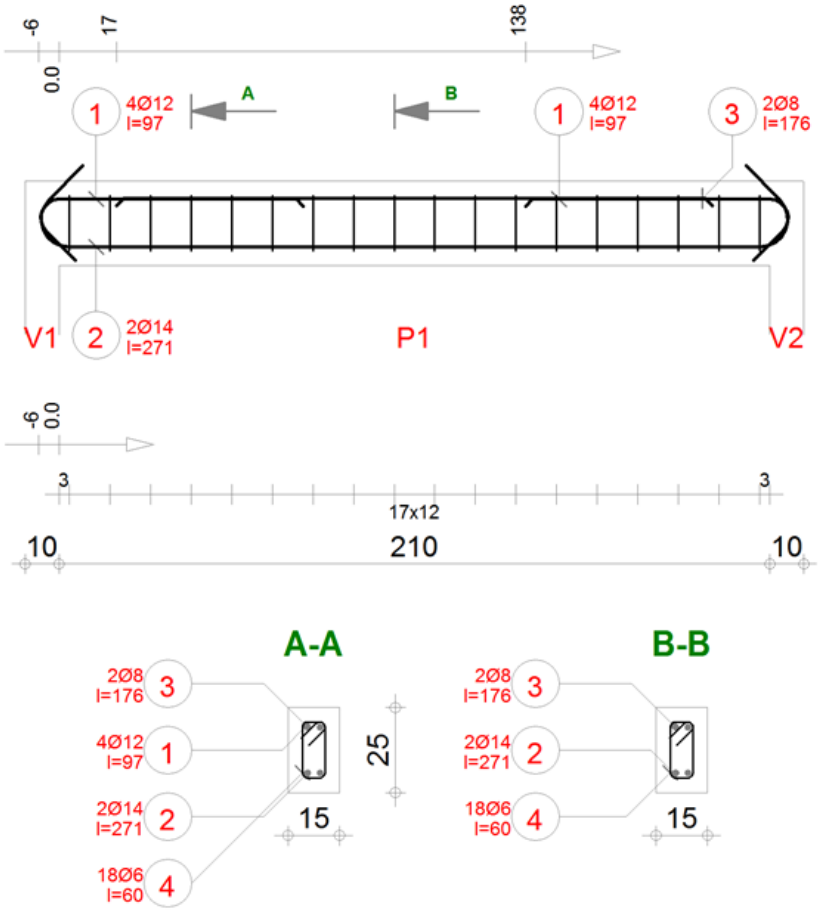

Figure 5: Reinforcement drawing (position, dimension, diameters) for the tested beams (tests `Beam1PO`, `Beam2PO`, `Beam3PsDSS` and `Beam4PsDB`).

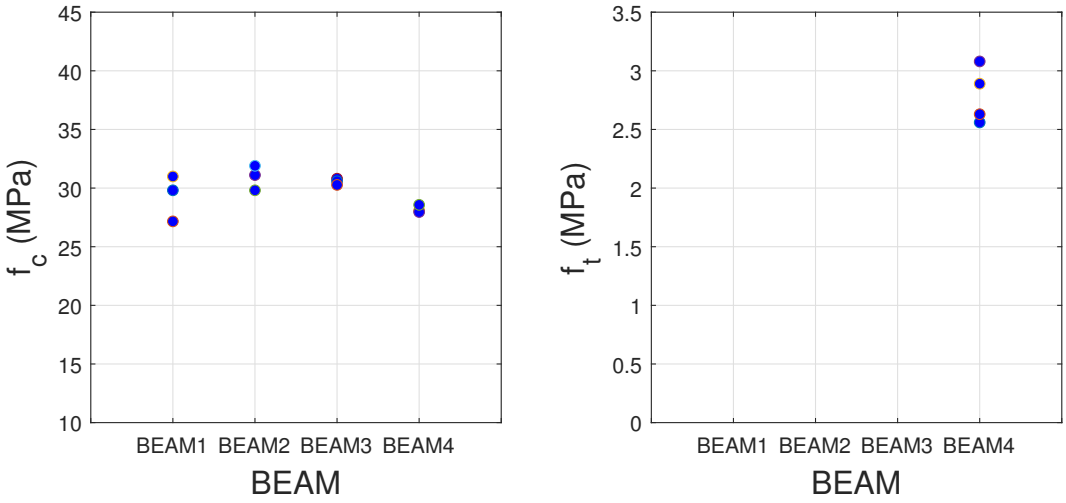

Figure 6: Mechanical properties of the beams' concrete. Strength in compression (f_c) and tension (f_t). 3 samples tested in compression for each beam. 4 samples tested in tension for beam n^{o}4.

gion Of Interest (ROI), located at the beam's mid-span (Figure 7). The open-source software used to carry out the DIC analysis is Ufreckles[1]. To record images during the tests, a Imager M-lite 5M (LaVision) camera is used (CMOS sensor - 5 MPix - 2464×2056 - 8bits - 3.45 µm^2 pixel size). The lens is a Tamron 1/1.12 25 mm F/1.8 M112FM25 ϕ27.

2.3.3 Pushover tests

To obtain the mechanical response of the tested RC members (stiffness and strength), two RC beams (so-called `Beam1PO` and `Beam2PO`) are loaded by pushover under three-point bending conditions. A constant velocity is applied to the specimens. To assess the loading rate dependency, two pushover are performed with two different loading rates (`Beam1PO` at 10 mm.s^{-1}, `Beam2PO` at 0.032 mm.s^{-1}).

2.3.4 PsD test without sub-structuring

In a sake of simplicity, a PsD test without sub-structuring (so called `Beam4PsDB`) is performed before the PsD test with sub-structuring (test `Beam3PsDSS`). The

[1] https://github.com/jrethore/ufreckles

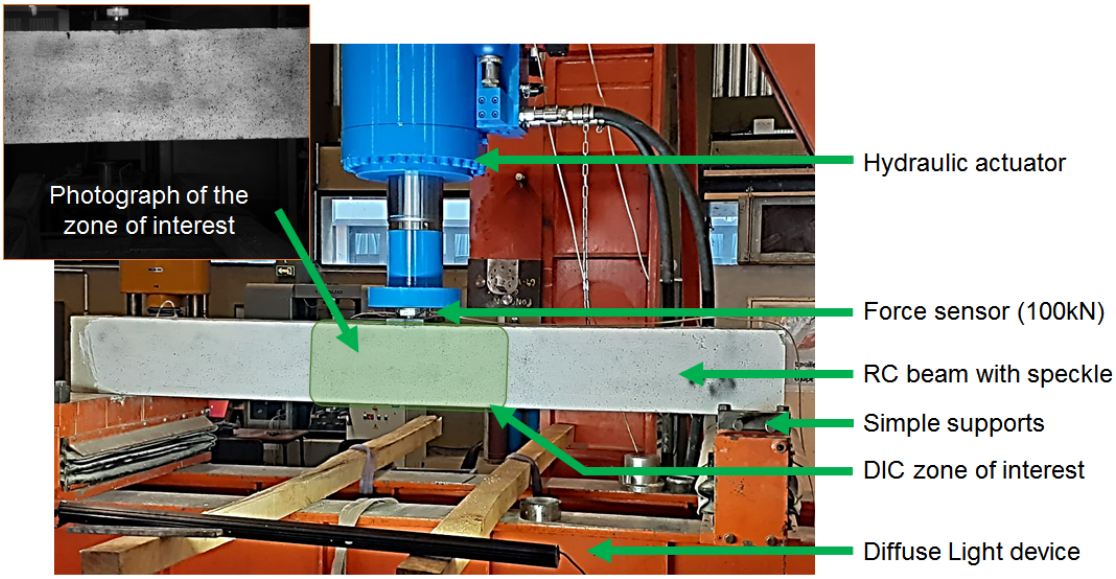

Figure 7: Experimental setup for each tested beams. DIC analysis is performed right under the load application (green zone).

objective is to obtain results from a simpler PsD configuration to assess only the RC beam's nonlinear behavior without sub-structure interaction.

The beam's mechanical response is analyzed considering a "virtual" concentrated mass $M_p = 4500$ kg (Figure 4a) at the beam's mid-span. At time zero, the beam is instantly loaded with a constant force coming from the added mass's weight.

The dynamic response of the system, *i.e.* the inertial force contribution, is obtained through the PsD algorithm. In that case, the stiffness and mass matrices are defined such as $\mathbb{M} = M_p$, $\mathbb{K}^I = K^I = 5.7 \cdot 10^6$ N.m^{-1}, $\xi = 5\%$, $f_1 = \sqrt{K^I/M_p}$, $\omega_1 = 2\pi f_1$ and $\omega_2 = 0$, f_1 being the first and only eigenfrequency. K^I is the initial stiffness assessed from experimental measurements. The timestep of the integration scheme equals 0.001 s.

2.3.5 PsD test with sub-structuring

The PsD testing with sub-structuring (so called `Beam3PsDSS`) is performed by simulating all the structure with beam finite elements based on *Euler-Bernoulli* kinematic. Only the first lower beam corresponds to the tested part (Figure 4b). That way, the effect of the internal efforts redistribution into

the rest of the structure can be described. The interface between the tested part and the simulated part is located at the vertical DOF corresponding to the mid span of the tested beam.

In a sake of simplicity, the simulated part is supposed elastic and because the bearing loss is due to the lower central post removal, the overall response can be assumed symetric. The mesh of the simulated part is depicted in figure 8a. The *Young* modulus of the simulated beams is $E = 21$ GPa and its density $\rho = 2500$ kg/m^3. Internal hinges and additional masses (2800 kg each) are implemented into the frame to increase the loading applied onto the tested beam (Figure 4b). The *Rayleigh* damping ratio is set at 5% and is applied on the first and fifth eigen modes of the simulated part.

The boundary conditions of the tested beam ends are simply supported (no vertical displacement and no bending moment) and disconnected from the rest of the portal frame. The complexity to built a representative connexion is still a limitation of the approach because it involves six additional hydraulic jacks to be able to impose the cross-section's kinematic at the tested beam's ends (3DOF each). However, because of the post's axial rigidity (compared to the beams's bending rigidity), it can be supposed in a first approximation, that vertical displacements of the beam ends can be neglected compared to the mid span displacement.

2.4 Multifiber numerical model

In order to simulate the pushover (`Beam1PO` and `Beam2PO`) and PsD tests (`Beam3PsDSS` and `Beam4PsDB`), the tested beam is modelled with a multifiber beam finite element model (Mazars and Grange [2015]). Multifiber beam theory constitutes a good compromise between computational efficiency and refined description of localized physics phenomena related to the nonlinear response of the material considered. The latter is taken into account by discretizing the cross-section into fibers (Figure 9). The cross-section has 12 fibers along the depth of the beam and 2 along the orthogonal axis. Along its longitudinal axis, the beam is discretized with 10 beam finite elements based on *Timoshenko* kinematic assumptions (Kotronis and Mazars [2005]). Then, only the nonlinear behavior of the material along the longitudinal axis of the beam is described.

The concrete behavior law is based on the work of LaBorderie [1991]. It describes the effect of progressive microcracking responsible for the stiffness loss within the plain concrete. The model is able to account for the crack

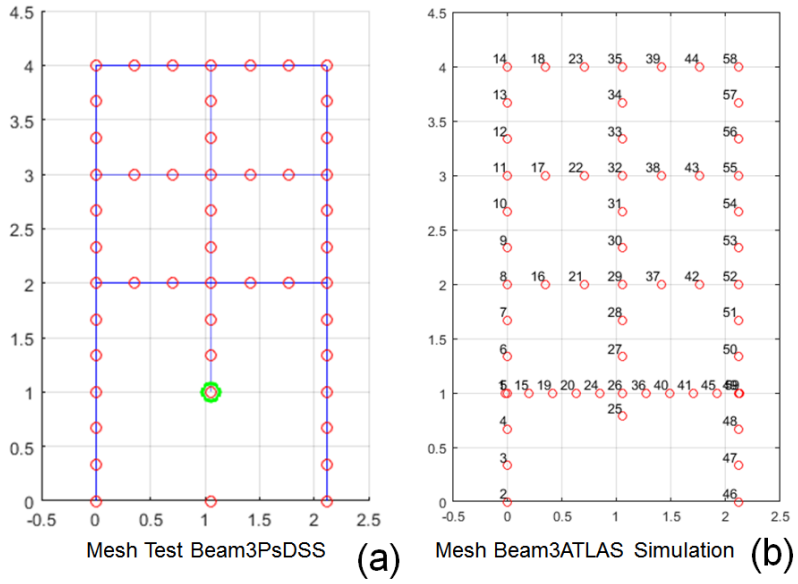

Figure 8: Meshes of the test `Beam3PsDSS` (the tested beam is not represented) where the green point corresponds to the connexion between the simulated and tested parts (a), and the multifiber finite element model based on ATL4S computational plateform (Grange [2009-2021]) (b). The red dots correspond to the nodes of the meshes.

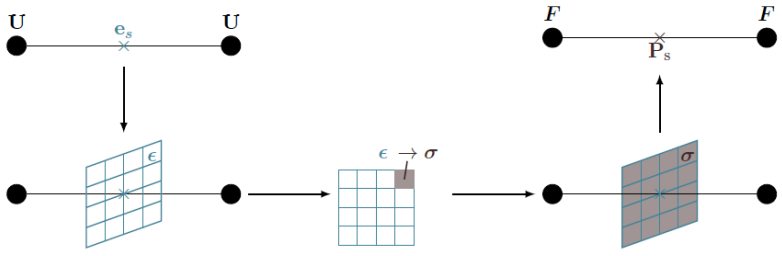

Figure 9: Multifiber theory principle (Kotronis and Mazars [2005], Capdevielle [2016]) : discretization of the cross-section and computation at the scale of each fiber with an *ad hoc* uniaxial behavior law.

Test	Stiffness k_{beam} (N.m^{-1})	Plateau F_{beam} (N)
`Beam1PO`	$5.40 \cdot 10^6$	$5.61 \cdot 10^4$
`Beam2PO`	$5.02 \cdot 10^6$	$5.61 \cdot 10^4$
`Beam4PsDB`	$6.47 \cdot 10^6$	$6.04 \cdot 10^4$
`Beam3PsDSS`	$4.61 \cdot 10^6$	-

Table 1: Beam's stiffnesses and maximal strength from pushover and cyclic tests.

closure effect (unilateral contact) under cyclic loads. The steel behavior law is based on a 1D model proposed by Menegotto and Pinto [1973]. The latter is a nonlinear hysteretic model for steel accounting for isotropic strain hardening effects. The simulations are performed within a dynamic framework where *Newmark* integration scheme is used with $\beta = 1/2$ and $\gamma = 1/4$ to guarantee unconditional stability and no numerical energy dissipation (Newmark [1959], Zienkiewicz and Taylor [1967], *etc.*).

Concerning the simulation of PsD test with sub-structuring (`Beam3PsDSS`), the simulated part is modelled exactly under the same assumptions. The latter is supposed elastic and is described with *Euler-Bernoulli* finite elements. The tested part is modeled by the previous multifiber model. The mesh adopted is presented in Figure 8b. Finally, for each simulation of PsD tests, damping ratios and values remain the same as the ones used in the tests.

3 Experimental and Numerical Results

3.1 Pushover tests

Four bending tests are performed. PsD tests are done under *quasi*-static conditions and thus are cyclic *quasi*-static tests which can be compared to pushover tests. Figure 10 represents force-displacement curves for the four tests. The force and the displacement are measured at mid span. The results underline the beams' macroscopic responses' variability. Experimental stiffnesses and plateaus corresponding to maximal strength are presented in Table 1. The largest stiffness variation is about 30% between `Beam4PsDB` and `Beam3PsDSS`, whereas the variation between maximal strength values is around 7%.

After calibration on the pushover test `Beam1PO`, the steel and concrete uni-

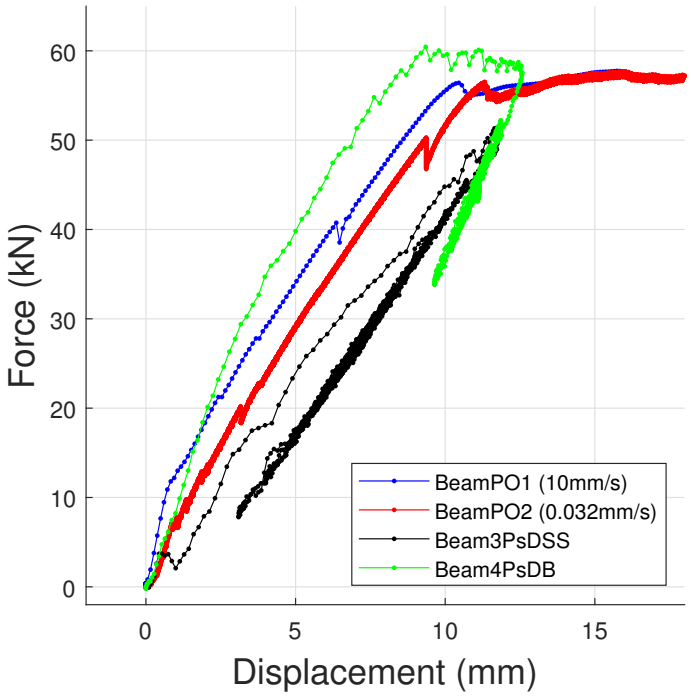

Figure 10: Force-Displacement responses of the tests `Beam1PO`, `Beam2PO`, `Beam3PsDSS` and `Beam4PsdB`.

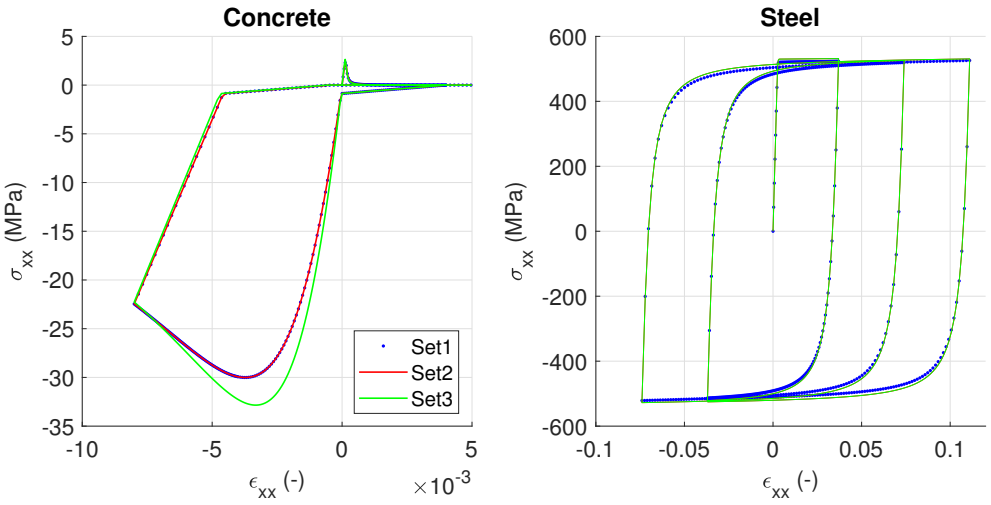

Figure 11: Uniaxial behavior laws for concrete (left) and steel (right) used within the multifiber model for parameters `set1`, `set2` and `set3` (*cf.* Table 2).

Parameter	Symbol	`Set1`	`Set2`	`Set3`	Unit
		CONCRETE			
Young's modulus	E_c	21	21	**25**	GPa
Poisson's coefficient	ν	0.2	0.2	0.2	-
Damage parameter	$Y0_1$	0.8375	0.8375	0.8375	-
Damage parameter	$Y0_2$	1000	1000	1000	-
Damage parameter	A_1	0.0021	0.0021	0.0021	-
Damage parameter	A_2	3.3e-6	3.3e-6	3.3e-6	-
Anelastic parameter	B_1	4.8	4.8	4.8	-
Anelastic parameter	B_2	1.219	1.219	1.219	-
Plain concrete damping	β_1	1.123e-5	1.123e-5	**1.0325e-5**	-
Damage concrete damping	β_2	-40e6	-40e6	-40e6	-
Stress crack closure	σ_{f1}	0.88	0.88	0.88	MPa
		STEEL REINFORCEMENT			
Young's modulus	E_s	200	200	200	GPa
Yield stress	f_y	520	**530**	**530**	MPa
Ultimate stress	f_u	530	**535**	**535**	MPa
Yield strain	f_y/E_c	0.0027	0.0027	0.0027	-
Ulimate strain	ϵ_u	0.11	0.11	0.11	-
Lower axial bar diameter	ϕ_{LOW}	14	14	14	mm
Upper axial bar diameter	ϕ_{UP}	8	8	8	mm
Axial bar excentricity along y axis	ex_y	69	**71**	**72**	mm

Table 2: Parameters used for the behavior laws (steel and concrete) within the multifiber model. Index 1 (resp. 2) is related to the tension (resp. compression) regim.

axial behaviors laws used within the multifiber model are depicted in Figure 11. Because of the variability of the tested beams, three sets of parameters are considered in order to get the parameters' effect on the beam's mechanical response. Table 2 summarizes the parameters used for each behavior laws.

Parameters `Set1` are chosen based on the material data coming from measurements (averaged concrete compressive strength of 30 MPa, and averaged tensile strength of 2.8 MPa). The yielding stress of the steel is set at 520 MPa. The longitudinal lower and upper reinforcements are placed according to the design (excentricity of $ex_y = 69$ mm with respect to the longitudinal axis). The effect of the bars excentricity is underlined with the parameters `Set2` ($ex_y = 71$ mm). In addition, steel yielding stress is slightly increased in order to get a higher final plateau. The parameters `Set3` are meant to fit the stiffness and strength of the test `Beam4PsDB`. Excentricity is further increased ($ex_y = 72$ mm), as well as concrete *Young*'s modulus ($E_c = 25$ GPa) and concrete compressive strength (33 MPa).

In the case of pushovers tests, a very good agreement is observed (Figure 12a). Effect of excentricity and concrete/steel paramaters can be observed on Figures 12b and 12c.

3.2 Without sub-structuring (`Beam3PsDB`)

The value of the "virtual" mass ($M_p = 4500\ kg$) has been chosen based on preliminary numerical simulations in order to ensure nonlinear response of the beam, whilst not exceeding its ultimate strength. As expected, significant damage is observed (concrete macrocraking and reinforced bars yielding).

Parameters `Set3` are used to reproduce the PsD test (`Beam3PsDB`) using ATL4S. The beam's modal response is well captured by the simulation. A good agreement can be observed between experimental and numerical results (Figure 13). Slight differences remain, relative to the parameters' calibration. The ATL4S model's stiffness is smaller, which accounts for the displacements' overestimation as well as the larger vibration period. The force plateau's occurence is very well reproduced.

3.3 With sub-structuring (`Beam4PsDSS`)

As a preliminary step, a modal analysis is carried out to check the numerical models's setups (`Beam3PsDSS` test and ATL4S model). In the case of the PsD

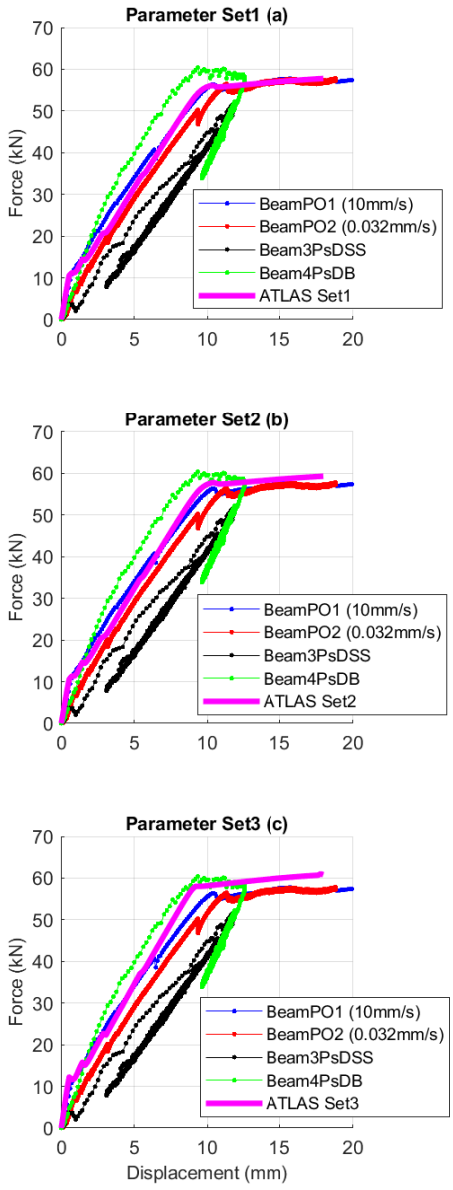

Figure 12: Comparisons of ATL4S multifiber models and experimental tests. Pushover in *quasi*-static (three-point bending) for the 3 parameter sets (`Set1` (a), `Set2` (b) and `Set3` (c)).

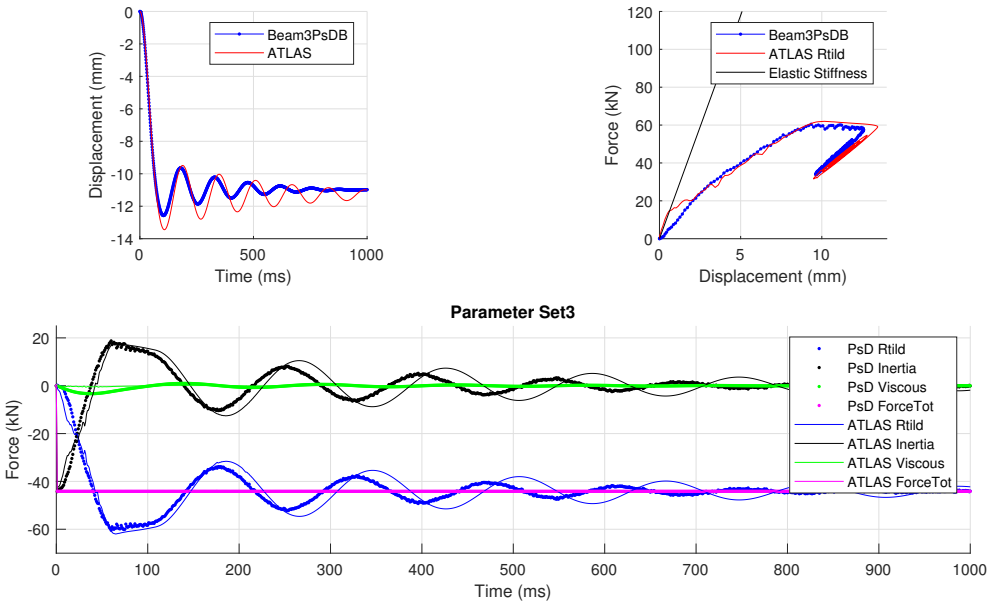

Figure 13: ATL4S multifiber model (`Set3`) and PsD test `Beam4PsDB` comparison - time history of mid-span displacement and force contributions (static, inertial, viscous, loading).

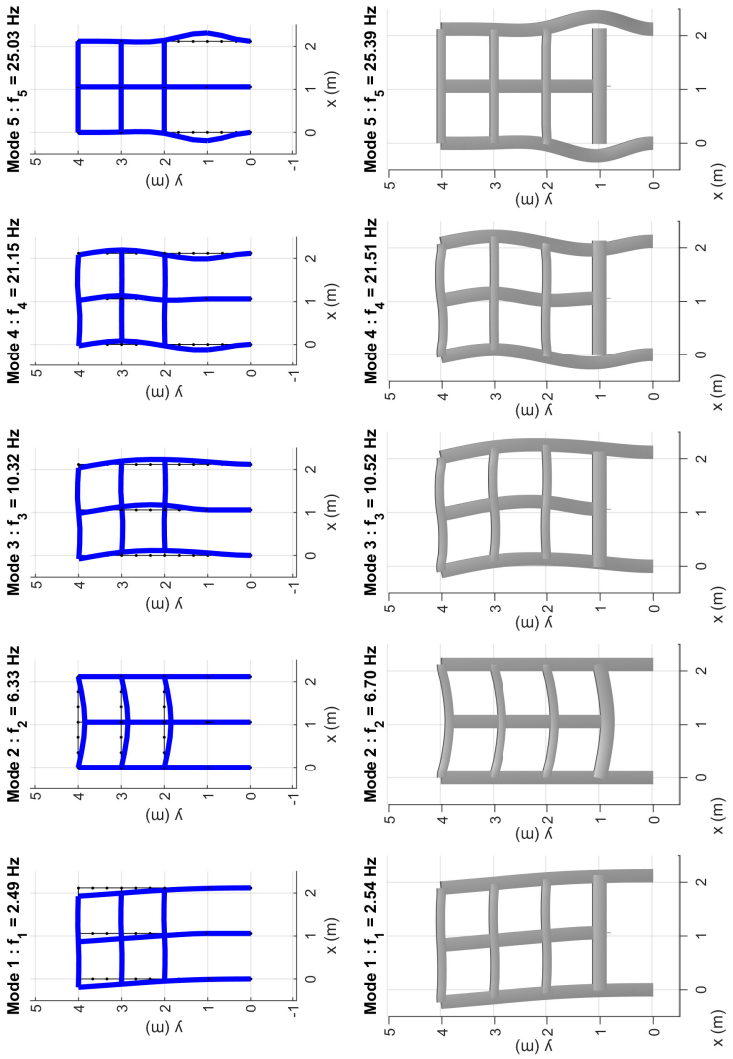

Figure 14: Modal analysis comparison between ATL4S model (lower row) and a the PsD test `Beam3PsDSS` (upper row) where the tested part is replaced by an elastic spring having the elastic bending stiffness of the tested RC beam.

Eigenmode	Frequency `Beam3PsDSS`	Frequency ATL4S model	Relative variation
1	2.49 Hz	2.54 Hz	2.0%
2	6.33 Hz	6.70 Hz	5.8%
3	10.3 Hz	10.5 Hz	2.0%
4	21.2 Hz	21.5 Hz	1.4%
5	25.0 Hz	25.4 Hz	1.6%

Table 3: Comparison of the first five eigenfrequencies of `Beam3PsDSS` and its twin ATL4S multifiber model.

test `Beam3PsDSS`, the modal analysis is performed by considering the tested RC beam's as a vertical elastic spring (Figure 14, upper row) having an elastic stiffness calibrated on the bending stiffness coming from experimental data ($k_{spring} = 5.34 \cdot 10^{-6}$ N.m^{-1}). The latter value is the averaged macroscopic bending stiffness of the four tested beams (Figure 10). In the case of the ATL4S model, the *Young*'s modulus of the multifiber beam elements has been set (5660 MPa) to exhibit the same apparent bending stiffness (k_{spring}) of the tested RC beams. Figure 14 and Table 3 underline the very good agreement between the PsD test `Beam3PsDSS` and its twin numerical model.

Then, the PsD test (`Beam3PsDSS`) is carried out and time histories are compared using parameters `Set1`. Figure 15 shows very good agreement between experimental and numerical results. Due to its loading and its boundary conditions, the structure responses mostly along its second eigenmode. Vibration frequency and the deformed shape agree very well. In addition, the effect of internal effort redistribution can be noted. Indeed, the tested beam does not develop significant damage compared to the `Beam4PsDB` test, due to load repartition within the upper stories.

3.4 Cracking patterns

For both PsD tests, Digital Image Correlation (DIC) is performed to follow the time evolution of cracking pattern right at the beam's mid-span. A picture is taken every 10 ms (resp. 5 ms) for `Beam3PsDSS` test (resp. `Beam4PsDB` test). The time mentioned is the numerical time of the PsD algorithm, and not the experiment's physical time.

In order to capture cracks pattern through DIC, the correlation error

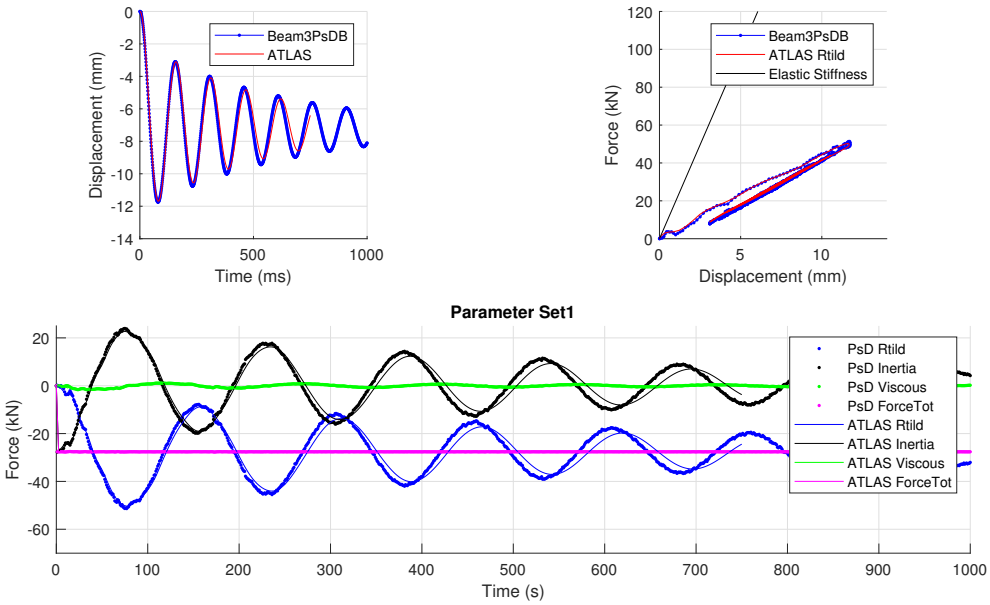

Figure 15: PsD test `Beam3PsDSS` and ATL4S model (parameters `Set1`) comparison - time history of mid-span displacement and force contributions (static, inertial, viscous, loading)

field is considered. Kinematic field interpolation is based on images divided into four noded quadrilateral finite elements (size 40 Pix $\times$ 40 pix). Initial correlation error before loading (measurement noise) is on average lower than 1%. In order to detect cracks, the correlation error threshold used is equal to 15%.

In the case of `Beam4PsDB`, Figure 16 suggests that the main cracks' development (vertical cracks due to bending response) is reached after the first displacement peak. After the first peak, the crack pattern does not change anymore and no crack closure can be observed. For the `Beam3PsDSS` test, analogous crack distribution is observed (Figure 17). However, opening and re-closure of the cracks through time is noted. This underlines that the beam's full capacity (reaching of strength plateau) is not completely consumed.

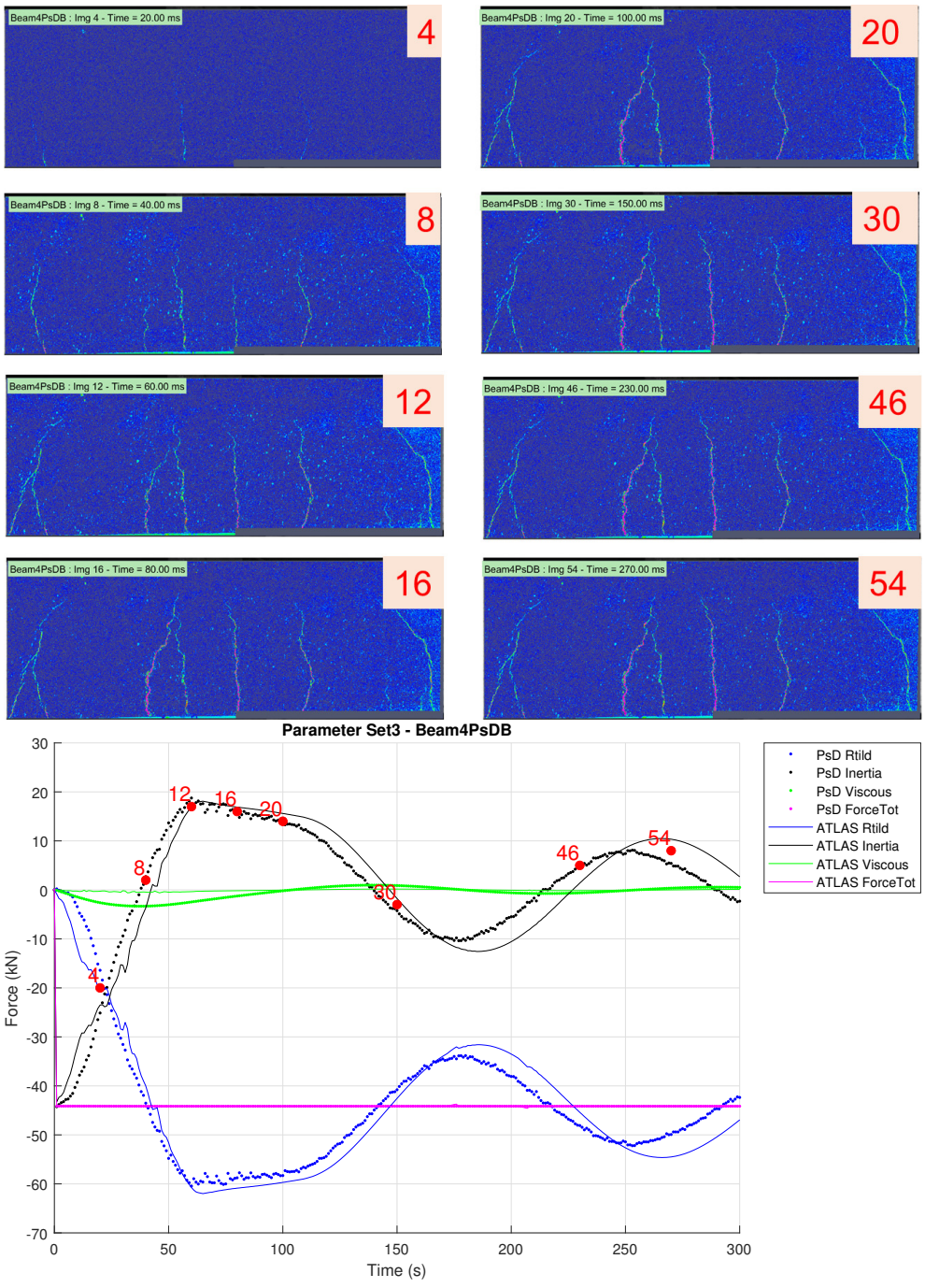

Figure 16: Time history of cracks spatial distribution - `Beam4PsDB` test - mid-span. Image number (red dot) is reported on the time history to identify the instant of the photo capture.

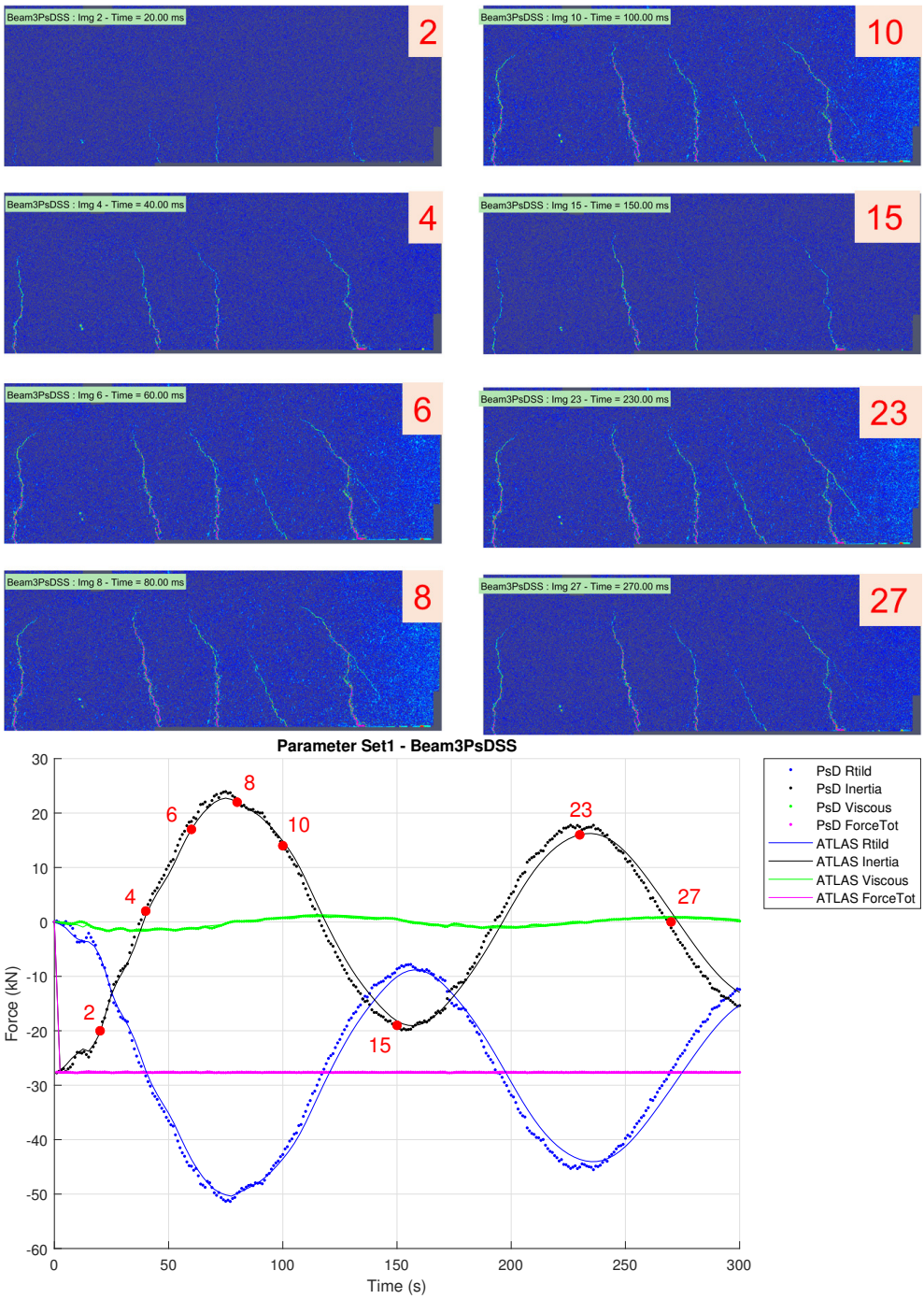

Figure 17: Time history of cracks spatial distribution - `Beam3PsDSS` test - mid-span. Image number (red dot) is reported on the time history to identify the instant of the photo capture.

4 Conclusion

A new way to assess the effect of loss of bearing capacity on civil engineering is proposed. The method is based on Pseudo-Dynamic testing coupled with sub-structuring technique. A very good agreement between the nonlinear multifiber models and the experimental tests is observed. Once calibrated, the same parameter set can be used to reproduce the *quasi* static and dynamic responses of the considered structures with or without sub-structuring. In addition, the pushovers tests validate the possibility to use a PsD approach. Indeed, for this PC senario, the material's properties do not exhibit a dependance to the strain-rate. It demonstrates the robustess and the interest to use this kind of approach in this context.

One of the advantage of the approach is the experimental setup's reduced cost and complexity. It allows to test only the most affected part of the structure and accounts for the effect of the overall structure without having to test all the structure. Performing an exprimental testing on the critical part allows to better capture the nonlinear response without having to use complex nonlinear models which can be tricky to calibrate if severe nonlinear response is expected. Another very important point is the ability of the PsD approach to describe the dynamic response of the structure by accounting for the inertial forces. In that sense, full scale analysis are thus more feasible and representative. Moreover, only *quasi* static loading are needed to carried out the PsD tests and thus it allows to use classic intrumentation at a low acquisition frequency and improves the safety and the controlability of the tests.

For now, the simulated part has been supposed elastic but extension to nonlinear response is rather straightforward. Next step will be to used nonlinear multifiber model to describe the simulated part which will give the possibility to assess the propagation of moderate damages to the rest of the structure. Another point concerns the boundary conditions between the tested and simulated parts. In order to better describe the potential interaction between those two domains, a work is under progress to improve the supports especially at the ends of the tested beam. The objective is to use additional hydraulic jack to account for the interaction between the beam and the posts. The evolution of the overall stiffness of the structure during the degradation progress can have significant effect on the modal response. Additional measurement techniques can be used (optic fiber, ambient vibration measurement, *etc.*) to better analyze the involved phenomena.

From a numerical point of view, new coupling algorithms can be tested to improve the computation efficiency by using HATI (Heterogeneous and Asynchronous Time Integrations) approaches (Grange and Bertrand [2021]). That way, the experimental part would be describe with an explicit scheme (small timestep) and the simulated part would be described with implicit scheme (large timestep).

Finally, other technologies and materials can be considered (steel, wooden frame, *etc.*) and redundancy aspects can also be explored to assess the efficiency of new technologies. Because the PsD approach accounts for the inertial forces, the analysis of DAF can be readily considered.

5 Acknowledgements

The support of INSA Lyon is gratefully acknowledged. In addition, this work has been partially developed within the framework of the federative project I-RISK (L'offre de solutions au traitement des risques naturels) co-funded by the European Union (FEDER) and "La région Auvergne-Rhône-Alpes" which aims at proposing innovative solutions for natural hazards mitigation.

References

T. Krauthammer, R. Hall, Woodson S., Baylot J., Hayes J., and Sohn Y. Development of progressive collapse analysis procedure and condition assessment for structures. In DC Multihazard Mitigation Council of the National Institute of Building Sciences: Washington, editor, *National Workshop on Prevention of Progressive Collapse in Rosemont*, 2003.

M. Sasani and J. Kropelnicki. Progressive collapse analysis of an rc strcuture. *Struct. Design Tall Spec. Build.*, 17:757–771, 2008.

O. Yagob and K. Galal. Progressive collapse of reinforced concrete structures. *Structural Engineering and Mechanics*, 32(6):771–786, 2009.

Z. Bazant and Y. Zhou. Why did the world trade center collapse?—simple analysis. *Journal of Engineering Mechanics*, 128(1), 2002.

J. Adam, F. Parisi, J. Sagaseta, and X. Lu. Research and practice on progressive collapse and robustness of building structures in the 21st century. *Engineering Structures*, 173:122–149, 2018.

F. Kiakojouria, V. DeBiagi, B. Chiaia, and M. Sheidaiia. Progressive collapse of framed building structures: Current knowledge and future prospects. *Engineering Structures*, 206:110061, 2020.

Y. Tian, K. Lin, X. Lu, L. Zhang, Y. Li, and H. Guan. Experimental and theoretical study of seismic and progressive collapse resilient composite frames. *Soil Dynamics and Earthquake Engineering*, 139, 2020.

B. Meng, L. Li, W. Zhong, Z. Tan, and Q. Du. Improving anti-progressive collapse capacity of welded connection based on energy dissipation cover-plates. *Journal of Constructional Steel Research*, 2022.

U. Starossek. Typology of progressive collapse. *Engineering Structures*, 29: 2302–2307, 2007.

W. Yi, F. Yi, and Y. Zhou. Experimental studies on progressive collapse behavior of rc frame structures: Advances and future needs. *International Journal of Concrete Structures and Materials*, 15(31):23p, 2021.

I. Alshaikh, B. Bakar, E. Alwesabi, and H. Akil. Experimental investigation of the progressive collapse of reinforced concrete structures: An overview. *Structures*, 25:881–900, 2020.

M. Byfield, W. Mudalige, C. Morison, and E. Stoddart. A review of progressive collapse research and regulations. *Structures and Buildings*, 167: 447–456, 2014.

M. ElHajjDiaba, A. Orcesi, C. Desprez, and J. Bleyer. A progressive collapse modelling strategy coupling the yield design theory with non-linear analysis. *Engineering Structures*, 241, 2021.

AmericanStd. Unified facilities criteria, design of buildings to resist progressive collapse, 2009.

AmericanStd. Alternate path analysis & design guidelines for progressive collapse resistance, 2016a.

M. Sasani and S. Sagiroglu. Progressive collapse resistance of hotel san diego. *Journal of Structural Engineering*, 134(3), 2008.

B. Song, H. Sezen, and K. Giriunas. Experimental and analytical assessment on progressive collapse potential of two actual steel frame buildings. In *Structures Congress*, 2010.

T. Wang, Q. Chen, H. Zhao, and L. Zhang. Experimental study on progressive collapse performance of frame with specially shaped columns subjected to middle column removal. *Shock and Vibration*, page 13p, 2016.

S. Shan, S. Li, S. Xu, and L. Xie. Experimental study on the progressive collapse performance of rc frames with infill walls. *Engineering Structures*, 111:80–92, 2016.

W. Yi, Q. He, Y. Xiao, and S. Kunnath. Experimental study on progressive collapse-resistant behavior of reinforced concrete frame structures. *ACI Structural Journal*, 105(4):433–439, 2008.

H. Lew, Y. Bao, F. Sadek, J. Main, S. Pujol, and M. Sozen. An experimental and computational study of reinforced concrete assemblies under a column removal scenario. Nist technical note 1720, National Institute of Standards and Technology, 2011.

F. Sadek, J. Main, H. Lew, and Y. Bao. Testing and analysis of steel and concrete beam-column assemblies under a column removal scenario. *Journal of Structural Engineering*, 137 (9):881–892, 2011.

Q. Kai and B. Li. Dynamic performance of rc beam-column substructures under the scenario of the loss of a corner column—experimental results. *Engineering Structures*, 42:154–167, 2012.

Q. Kai and B. Li. Performance of three-dimensional reinforced concrete beam-column substructures under loss of a corner column scenario. *Journal of Structural Engineering*, 139 (4):584–594, 2013.

Q. Kai and B. Li. Research advances in design of structures to resist progressive collapse. *Journal of Performance of Constructed Facilities*, 2014.

S. Orton and J. Kirby. Dynamic response of a rc frame under column removal. *J. Perform. Constr. Facil.*, 28, 2014.

C. Liu, T. Fung, and K. Tan. Dynamic performance of flush end-plate beam-column connections and design applications in progressive collapse. *Journal of Structural Engineering*, 2015.

A. Pham and K. Tan. Experimental study on dynamic responses of reinforced concrete frames under sudden column removal applying concentrated loading. *Engineering Structures*, 139:31–45, 2017.

M. Scalvenzi, S. Gargiulo, F. Freddi, and F. Parisi. Impact of seismic retrofitting on progressive collapse resistance of rc frame structures. *Engineering Failure Analysis*, 2022.

AmericanStd. Design of structures to resist progressive collapse (rev. 3)., 2016b.

EuropeanStd. Nf en 1991-1-7 (février 2007) : Eurocode 1 - actions sur les structures - partie 1-7 : Actions générales - actions accidentelles + amendement a1 (août 2014) (indice de classement : P06-117), 2014.

H. Wang, A. Zhang, Y. Li, and W. Yan. A review on progressive collapse of building structures. *The Open Civil Engineering Journal*, 8:183–192, 2014.

P. Pegon and A. Pinto. Pseudo-dynamic testing with substructuring at the elsa laboratory. *Earthquake Engng Struct. Dyn.*, 29:905–925, 2000.

A. Souid, A. Delaplace, F. Ragueneau, and R. Desmorat. Pseudodynamic testing and nonlinear substructuring of damaging structures under earthquake loading. *Engineering Structures*, 31:1102–1110, 2009.

H. Hilbert, T. Hughes, and R. Taylor. Improved numerical dissipation for time integration algorithms in structural dynamics. *Earthquake Engineering and Structural Dynamics*, 1977.

M. Nakashima and H. Kato. Experimental error growth behavior and error growth control in on-line computer test control method. Bri-report no.123, ministry of construction, Building Research Institute, 1987.

D. Combescure and P. Pegon. α-operator splitting time integration technique for pseudodynamic testing : Error propagation analysis. *Soil Dynamics and Earthquake Engineering,*, 1997.

S. Grange. Atl4s plateform (a tool and language for simplified structural solution strategy). Technical report, INSA Lyon, 2009-2021.

P. Kotronis and J. Mazars. Simplified modelling strategies to simulate the dynamic behaviour of rc walls. *Journal of Earthquake Engineering*, 9 (2): 285 – 306, 2005.

S. Capdevielle. *Introduction du gauchissement dans les elements finis multi-fibres pour la modélisation des structures en béton armé*. PhD thesis, ED IMEP2, 2016.

J. Mazars and S. Grange. Modeling of reinforced concrete structural members for engineering purposes. *Computers and Concrete*, 16(5):683–701, 2015.

C. LaBorderie. *Phenomenes unilateriaux dans un materiau endommageable modélisation et application á l'analyse de structures en béton*. PhD thesis, Université Pierre et Marie Curie, 1991.

M. Menegotto and P. Pinto. Method of analysis of cyclically loaded rc plane frames including changes in geometry and non-elastic behavior of elements under normal force and bending. Technical Report 13, Preliminary Report IABSE, 1973.

N. Newmark. A method of computation for strcutural dynamics. *Engineering Mechanics DIVISION*, 1959.

O. Zienkiewicz and R. Taylor. *The finite element method for solid and structural mechanics*. Elsevier Butterworth-Heinemann, 1967.

S. Grange and D. Bertrand. Implicit coupling of heterogeneous and asynchronous time-schemes using a primal approach based on velocity continuity at the subdomain interface. *Finite Elements in Analysis and Design*, 196, 2021. doi: https://doi.org/10.1016/j.finel.2021.103604.